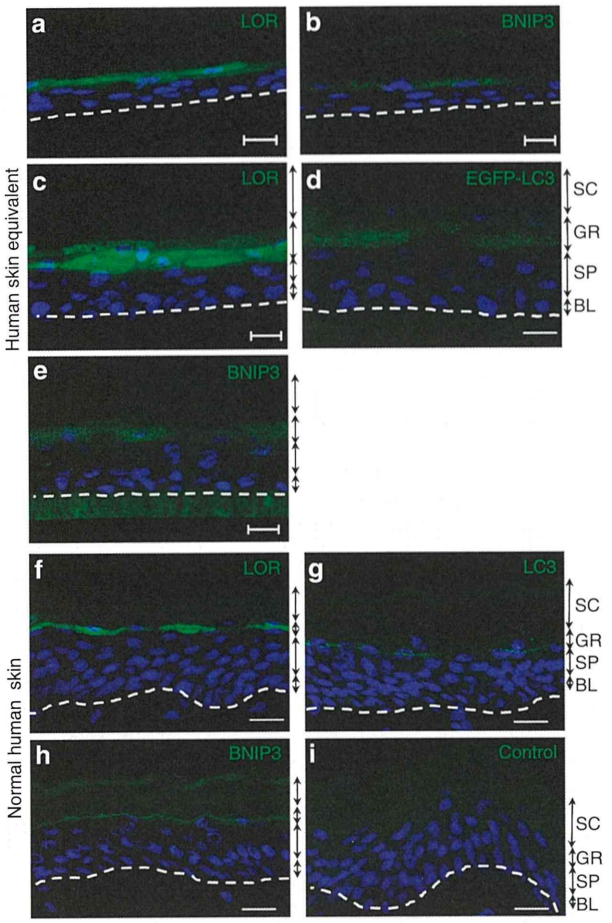

Figure 2. BNIP3 (BCL2 and adenovirus E1B 19-kDa-interacting protein 3) is expressed in the granular layer of the human epidermis. (**a**–**e**) Human skin epidermal equivalents were constituted from (**a**–**d**) normal human primary epidermal keratinocytes (HPEKs) or (**e**) HPEKs transfected with EGFP-LC3 by lentiviral vector. Cells were grown for (**a**, **b**) 18 days and (**c**–**e**) 24 days after exposure at the air–liquid interface. (**f**–**i**) Normal human skin epidermis. (**a**, **c**, **f**) Expression pattern of loricrin (LOR). (**b**, **e**, **h**) Expression pattern of BNIP3. (**i**) Control staining without BNIP3 antibody is shown. (**d**) Autophagosome formation determined by EGFP-LC3 puncta. (**g**) Endogenous expression pattern of LC3. The blue signals indicate nuclear staining. The dotted lines indicate (**a**–**e**) the boundary between the epidermis and the membrane or (**f**–**i**) the boundary between the epidermis and the dermis. Scale bars = 20 μm. BL, basal layer; GL, granular layer; SC, stratum corneum (cornified layer); SP, spinous layer.

that "sunburn-like cells" existed in BNIP3 knockdown epidermal equivalent (Figure 6a and b). We therefore hypothesized that BNIP3 might play a key role in the survival of epidermal keratinocytes. To evaluate this hypothesis, HPEKs were irradiated with 20 mJ cm^{-2} UVB. UVB irradiation triggered the formation of autophagosome that was significantly reduced by BNIP3 knockdown (Figure 6c–e). As shown in Figure 6f, UVB irradiation induced cleavage of caspase3 and BNIP3 expression. Intriguingly, knockdown of UVB-induced BNIP3 by RNAi further increased the amount of cleaved caspase3, suggesting that BNIP3 is required for the protection of keratinocytes from UVB-induced apoptosis (Figure 6f).

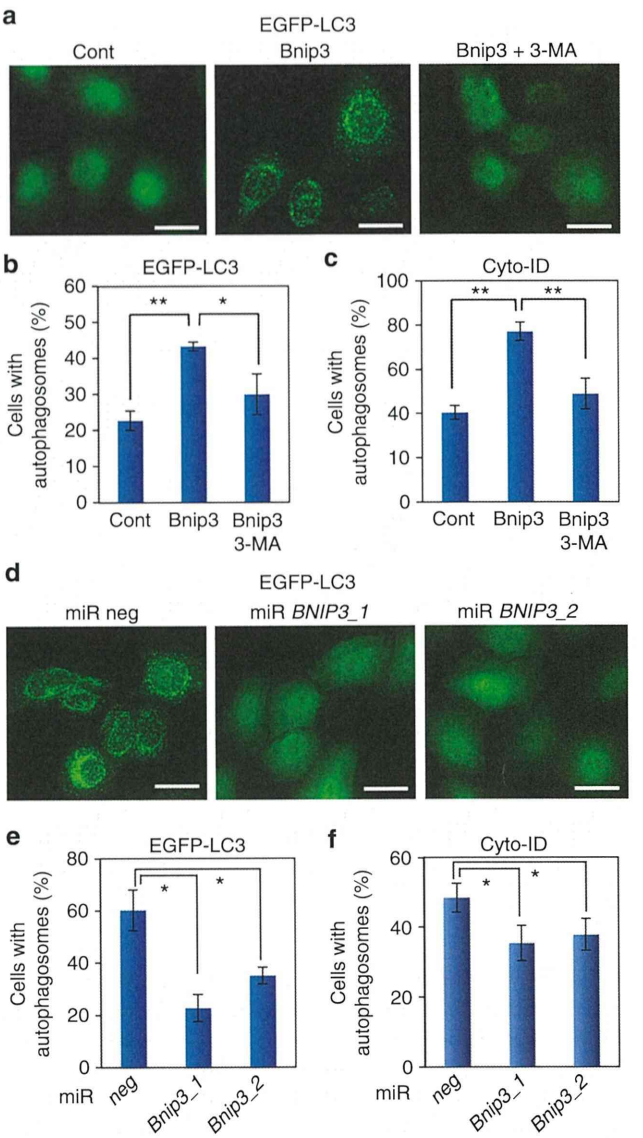

Figure 3. BNIP3 (BCL2 and adenovirus E1B 19-kDa-interacting protein 3) stimulates autophagy. (**a**, **b**) EGFP-LC3-expressing human primary epidermal keratinocytes (HPEKs) were transduced with DsRed (Cont) or BNIP3. As an inhibitor of autophagy, 3-methyladenine 3-MA (5 mM) was added. Cells were then stained with anti-EGFP at 24 hours after transduction. (**a**) EGFP-LC3 staining is shown in green. Scale bars = 20 μm. (**b**) The percentage of EGFP-LC3-positive cells with more than five puncta were quantified and are presented as the mean of three independent experiments ± SD. (**c**) HPEKs were transduced with DsRed (Cont) or BNIP3. As an inhibitor of autophagy, 3-MA (5 mM) was added. Autophagy induction was determined by Cyto-ID staining and quantified by flow cytometry. (**d**, **e**) EGFP-LC3-expressing HPEKs were transduced with miR *neg*, miR *BNIP3_1*, or miR *BNIP3_2* and induced to differentiate. Cells were then stained with anti-EGFP at 8 hours after differentiation induction. (**d**) EGFP-LC3 staining is shown in green. Scale bars = 20 μm. (**e**) The percentage of EGFP-LC3-positive cells with more than five puncta were quantified and are presented as the mean of three independent experiments ± SD. (**f**) HPEKs were transduced with miR *neg*, miR *BNIP3_1*, or miR *BNIP3_2* and induced to differentiate. Autophagy induction was determined by Cyto-ID staining and quantified by flow cytometry. All the data represent the average of three independent experiments ± SD. $^{**}P<0.01$; $^{*}0.01<P<0.05$.

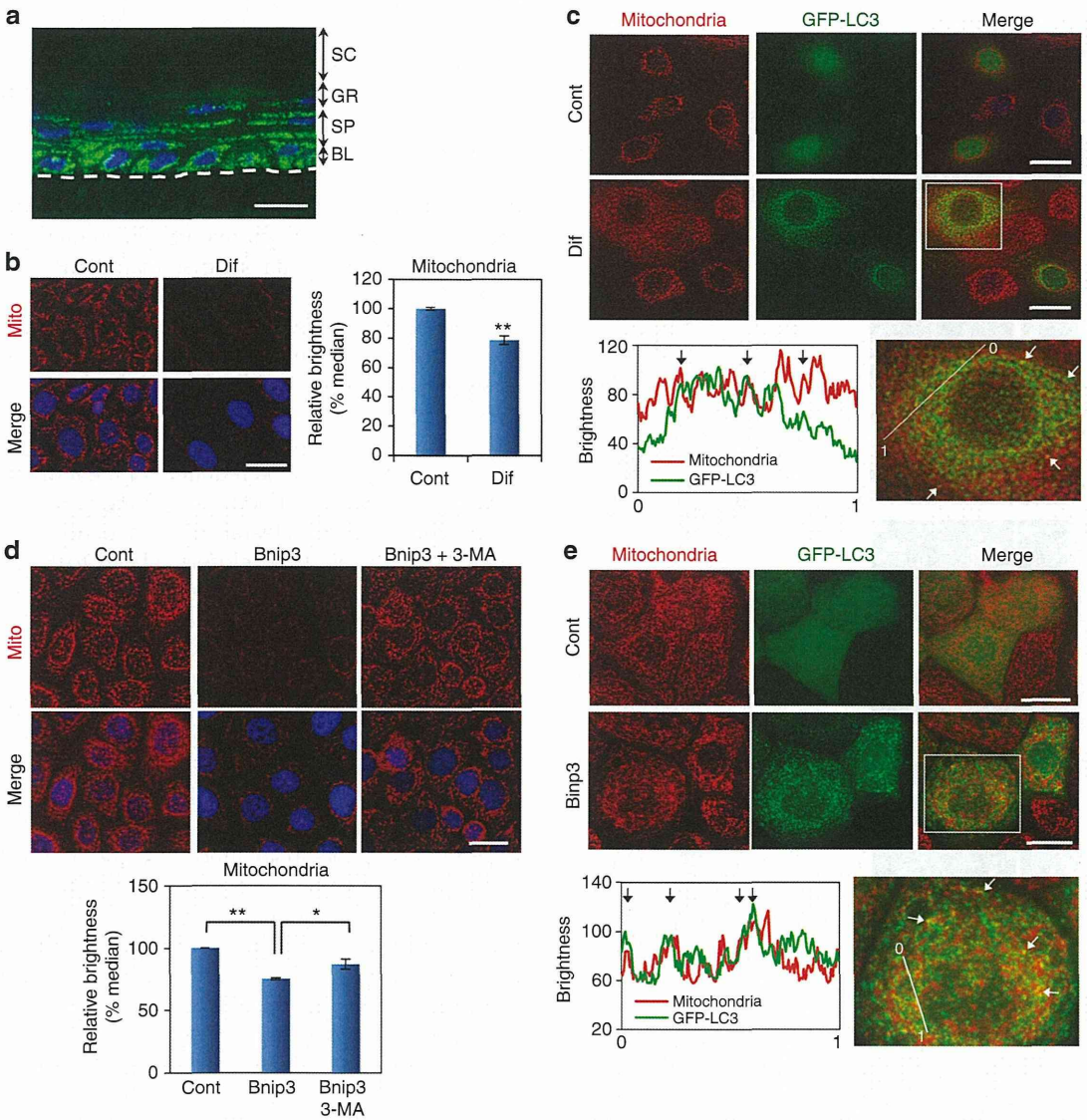

Figure 4. Autophagy stimulates mitochondrial degradation. (**a**) Distribution pattern of mitochondria. The blue signals indicate nuclear staining. The dotted lines indicate the boundary between the epidermis and the membrane. Scale bars = 20 μm. BL, basal layer; GL, granular layer; SC, stratum corneum (cornified layer); SP, spinous layer. (**b**) Nondifferentiated control (Cont) or differentiated human primary epidermal keratinocytes (HPEKs; Dif) were subjected to immunofluorescent staining 2 days after induction of differentiation. Mitochondrial staining is shown in red. The blue signals indicate nuclear staining. Scale bar = 20 μm. The graph indicates the percent of median brightness calculated by BZ Analyzer Software (Keyence) as the mean of three independent experiments ± SD. (**c**) EGFP-LC3-expressing HPEKs were differentiated. Cont or Dif were stained with anti-mitochondria (red) and anti-EGFP (green) 8 hours after induction of differentiation. Graph indicates the linescan analysis of the red and green fluorescent channels. Initial point of linescan is indicated as 0, and terminal point is indicated as 1. The arrows mark the colocalization of the two proteins. (**d**) HPEKs were transduced with enhanced green fluorescent protein (EGFP; Cont) or BNIP3 (BCL2 and adenovirus E1B 19-kDa-interacting protein 3). As an inhibitor of autophagy, 3-methyladenine 3-MA (5 mM) was added. Cells were then fixed and stained with anti-mitochondria 48 hours after transduction. Scale bar = 20 μm. The graph indicates the percent of median brightness calculated by BZ Analyzer Software (Keyence) as the mean of three independent experiments. $^{**}P<0.01$; $^{*}0.01<P<0.05$. (**e**) EGFP-LC3-expressing HPEKs were transduced with mock (Cont) or BNIP3. Cells were then fixed and stained with anti-mitochondria (red) and anti-EGFP (green) 24 hours after transduction. Graph indicates the linescan analysis of the red and green fluorescent channels. Initial point of linescan is indicated as 0, and terminal point is indicated as 1. The arrows mark the colocalization of the two proteins.

DISCUSSION

In this study, we demonstrated that BNIP3, a potent inducer of autophagy, plays a role in the terminal differentiation and maintenance of epidermal keratinocytes. It has been suggested that autophagy plays a role in the skin epidermis, but few attempts have been made to clarify the involvement of autophagy in skin epidermis.

We found that the HES1 transcriptional repressor directly suppressed BNIP3 expression in mouse epidermis and HPEKs (Figure 1). Moreover, our results revealed that BNIP3 was

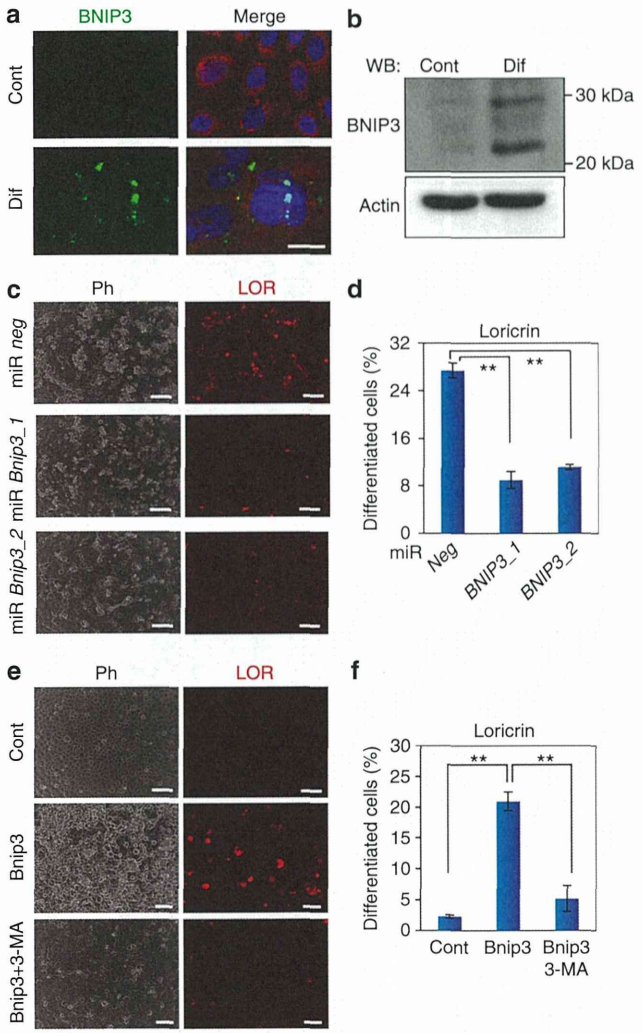

Figure 5. BNIP3 (BCL2 and adenovirus E1B 19-kDa-interacting protein 3) is required for the differentiation of keratinocytes *in vitro*. (**a**, **b**) Human primary epidermal keratinocytes (HPEKs) were differentiated and BNIP3 expression was observed. (**a**) Nondifferentiated control (Cont) or differentiated HPEKs (Dif) were subjected to immunofluorescent staining. BNIP3 staining is shown in green. Mitochondrial staining is shown in red. The blue signals indicate nuclear staining. Scale bar = 20 μm. (**b**) Western blot (WB) analysis. Proteins extracted from Cont or Dif were probed with anti-BNIP3 or anti-actin. (**c**, **d**) HPEKs were infected with adenoviral vectors expressing miR *neg*, miR *BNIP3_1*, or miR *BNIP3_2* followed by induction of differentiation. Cells were then immunostained with a loricrin antibody 9 days after transduction. (**e**, **f**) HPEKs were infected with adenoviral vectors expressing enhanced green fluorescent protein (EGFP; Cont) or BNIP3 and subjected to immunofluorescent staining against loricrin (LOR) 6 days after transduction. As an inhibitor of autophagy, 3-methyladenine 3-MA (5 mM) was added. Phase contrast images (Ph) and LOR staining are shown. Scale bars = 200 μm. (**d**, **f**) Percentages of LOR-positive differentiated cells were calculated by computerized image analysis. The data represent the average of three independent experiments ± SD. $^{**}P<0.01$.

expressed in the granular layers of mouse epidermis, its human skin epidermal equivalent, and its normal human skin epidermis (Figures 1 and 2). These data are consistent with our previous report showing that Hes1 is expressed in the spinous layers, where it represses the regulatory genes for differentiation to maintain the spinous cell fate (Moriyama *et al.*, 2008). Hence, it can be inferred that Bnip3 expression is suppressed in the spinous layers by Hes1, whereas it is upregulated in the granular layers where Hes1 expression is absent. In addition, our finding that BNIP3 is required for keratinocyte differentiation fits our idea that Hes1 represses certain regulatory genes to prevent the premature differentiation of spinous cells. Our *in vitro* data suggest that BNIP3 is involved in keratinocyte differentiation through autophagy (Figures 3–5). The mechanisms underlying the involvement of autophagy in keratinocyte differentiation remain elusive; however, considering that keratinocyte differentiation induced mitochondrial clearance and BNIP3 expression (Figure 4 and 5), BNIP3-induced autophagy may be responsible for the removal of mitochondria that may be required for the terminal differentiation of epidermal keratinocytes. During reticulocyte differentiation, programmed clearance of mitochondria induced by BNIP3L/Nix, a molecule closely related to BNIP3, has been reported to be a critical step (Schweers *et al.*, 2007). Therefore, keratinocytes likely possess the same differentiation mechanism that reticulocytes have, although further investigation will be required for elucidation.

In contrast to the results from differentiation in two-dimensional culture, we did not observe drastic differentiation defects in the BNIP3 knockdown human epidermal equivalent except for the existence of "sunburn-like cells" (Figure 6). This might be because of the incomplete suppression of BNIP3 in the BNIP3 knockdown keratinocytes, and/or might be because of the redundancy between BNIP3 and BNIP3L/Nix, a homolog of BNIP3, as we found in our preliminary study that Bnip3l is also expressed in the epidermis (data not shown). Although the phenotypes of BNIP3-null mice were published in 2007, these researchers found that BNIP3-null mice had no increase in mortality or apparent physical abnormalities (Diwan *et al.*, 2007). Generally, impairment of epidermal differentiation or skin barrier formation results in an obvious defect. Thus, BNIP3-null epidermis seems to exhibit subtle, if any, abnormalities. On the basis of these findings, the involvement of BNIP3 in epidermal differentiation must be investigated in the future. In-depth analysis of the BNIP3-null epidermis phenotype could help elucidate the role of BNIP3 in mouse epidermal differentiation.

Despite the lack of obvious differentiation defects in the human epidermal equivalent, our data showing that BNIP3 knockdown caused the appearance of "sunburn-like cells" is regarded as an example of apoptosis (Young, 1987), revealing a new role of BNIP3 in keratinocyte maintenance. Furthermore, requirement of BNIP3 for protection from UV-induced apoptosis was confirmed in two-dimensional keratinocyte cultures (Figure 6e). The underlying mechanism of this prosurvival function of BNIP3 in keratinocytes remains unclear; however, previous reports have demonstrated that hypoxia-induced autophagy through BNIP3 is critical for the prosurvival process (Bellot *et al.*, 2009). Recently, it has been reported that UVA induces autophagy to remove oxidized phospholipids and protein aggregates in epidermal keratino-

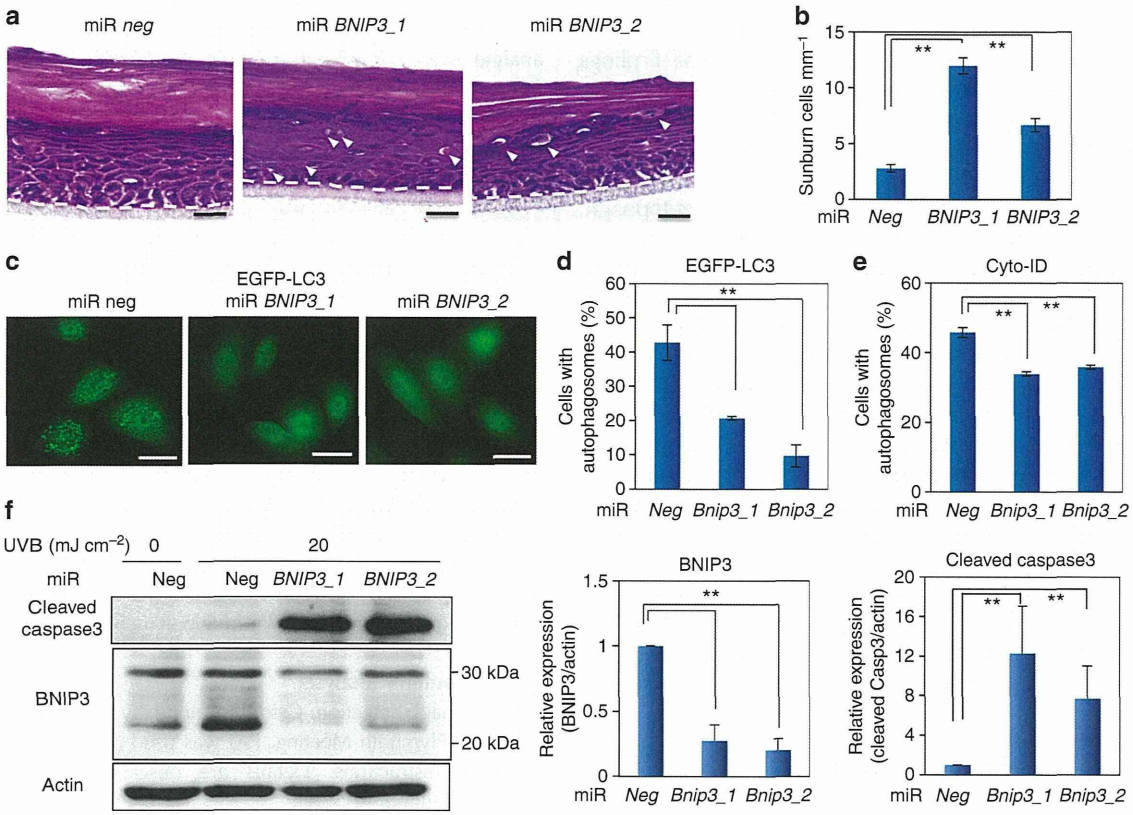

Figure 6. BNIP3 (BCL2 and adenovirus E1B 19-kDa-interacting protein 3) promotes cell survival in the reconstituted epidermis and keratinocytes. (**a**) Morphology of the human skin epidermal equivalents from human primary epidermal keratinocytes (HPEKs) infected with lentivirus expressing miR *neg*, miR *BNIP3_1*, or miR *BNIP3_2*. Arrowheads indicate sunburn-like cells. (**b**) The number of sunburn-like cells per mm was counted and plotted as the means of 10 sections ± SD. (**c–e**) HPEKs were infected with adenovirus expressing miR *neg*, miR *BNIP3_1*, or miR *BNIP3_2*, and irradiated with UVB. (**c**) Cells were stained with anti-EGFP at 8 hours after UVB irradiation. (**d**) The percentage of EGFP-LC3-positive cells with more than five puncta were quantified and are presented as the mean of three independent experiments ± SD. (**e**) Autophagy induction was determined by Cyto-ID staining and quantified by flow cytometry. The data represent the average of three independent experiments ± SD. (**f**) Cells were subjected to western blot analysis at 8 hours after irradiation. The blot shown is representative image of three independent experiments. Graphs indicate relative band intensities as determined by ImageJ software and plotted as the means of three independent experiments. Scale bars = 20 μm. $^{**}P<0.01$.

cytes (Zhao *et al.*, 2013). Because our data indicate that UVB-induced autophagy is mediated by BNIP3 (Figure 6c and d), it is possible that autophagy induced by BNIP3 also plays a role in the maintenance of keratinocytes. Further analysis is required to confirm these results.

UV-induced apoptotic cells appear within 12 hours and are predominately located in the suprabasal differentiated keratinocyte compartment of human skin (Gilchrest *et al.*, 1981). Moreover, differentiated keratinocytes appear to be most sensitive to the UV light that induces p53-dependent apoptosis (Tron *et al.*, 1998). Tron *et al.* (1998) demonstrated that differentiated keratinocytes in p53-null mice exhibited only a small increase in apoptosis after UVB irradiation compared with the increase observed in normal control animals (Tron *et al.*, 1998). Interestingly, because p53 has been reported to directly suppress BNIP3 expression (Feng *et al.*, 2011), BNIP3 might be abundantly upregulated in suprabasal cells in p53-null animals, resulting in the resistance to UVB-induced apoptosis. Indeed, our preliminary study showed that p53 knockdown enhanced UV-induced BNIP3 expression in HPEKs (data not shown). Therefore, BNIP3 expression in suprabasal cells appears to be important for the protection of differentiated keratinocytes from normal environmental stress such as weak UV exposure *in vivo*.

A recent report on a role for autophagy in epidermal barrier formation and function was identified in *atg7*-deficient mice (Rossiter *et al.*, 2013). The authors showed that autophagy was constitutively active in the suprabasal epidermal layers as we report in this study (Figure 2). However, in contradiction to our results, the authors concluded that autophagy was not essential for the barrier function of the skin. This may be because of the presence of an alternative Atg5/Atg7-independent autophagic pathway (Nishida *et al.*, 2009) in the epidermis. This Atg5/Atg7-independent pathway is also independent of LC3, but forms Rab9-positive double-membrane vesicles. Moreover, protein degradation via this pathway is inhibited by 3-MA and is dependent on Beclin 1. Our data demonstrate that: (1) BNIP3 induced the formation of

EGFP-LC3 puncta (Figure 4) and (2) 3-MA significantly diminished the formation of GFP-LC3 puncta and keratinocyte differentiation induced by BNIP3 (Figure 5). These findings suggest that BNIP3 in the epidermis induced both conventional and Atg5/Atg7-independent autophagy. Intriguingly, GFP cleaved from GFP-LC3 also accumulates in the *Atg7*-deficient epidermis (Rossiter *et al.*, 2013), thereby demonstrating the existence of an alternative autophagic pathway (Juenemann and Reits, 2012) in the epidermis. Further investigation will be required to determine whether Beclin 1 and Rab9 are indispensable for the BNIP3-induced autophagy and subsequent differentiation of keratinocytes.

In summary, our data reveal that expression of BNIP3 in granular cells induces autophagy and is involved in the terminal differentiation and maintenance of skin epidermis. Studies on the involvement of autophagy in skin epidermis have attracted considerable attention recently. In addition, increasing evidence suggests the involvement of BNIP3 in the differentiation of several cell types, including oligodendrocytes (Itoh *et al.*, 2003), osteoclasts (Knowles and Athanasou, 2008), and chondrocytes (Zhao *et al.*, 2012); however, the precise role of BNIP3 in this process remains to be investigated. Our study thus provides new insights into the functions of BNIP3 in differentiation and homeostasis.

MATERIALS AND METHODS

Histology and immunofluorescent analysis

Samples and embryos were fixed in 4% paraformaldehyde, embedded in optimal cutting temperature compound, frozen, and sectioned at 10 μm. Sections were then either subjected to hematoxylin and eosin staining or immunohistochemical analysis as previously described (Moriyama *et al.*, 2006). Details are described in Supplementary Materials Online.

Cell culture

HPEKs were purchased from CELLnTEC (Bern, Switzerland) and maintained in CnT-57 (CELLnTEC) culture medium according to the manufacturer's protocol. For induction of differentiation, the medium was changed to CnT-02 (CELLnTEC) at confluent monolayers of HPEKs, followed by adding calcium ions to 1.8 mM. The generation of human skin equivalents was performed using CnT-02-3DP culture medium (CELLnTEC) according to the manufacturer's protocol.

Design of artificial microRNAs and plasmid construction

Oligonucleotides targeting a human BNIP3 sequence compatible for use in cloning into BLOCK-iT Pol II miR RNAi expression vectors (Invitrogen, Carlsbad, CA) were obtained using the online tool BLOCK-iT RNAi Designer. The oligonucleotide sequences used in this study are shown in Supplementary Table S1 online. Cloning procedures were performed following the manufacturer's instructions.

Adenovirus and lentivirus infection

Adenoviruses expressing EGFP, Hes1, BNIP3, and miR *BNIP3* were constructed using the ViraPower adenoviral expression system (Invitrogen) according to the manufacturer's protocol. Lentivirus expressing EGFP-LC3 (from Addgene plasmid 21073, Cambridge, MA) and miR *BNIP3* plasmid was constructed and used to infect keratinocytes as previously described (Moriyama *et al.*, 2012; Moriyama *et al.*, 2013).

RNA extraction, complementary DNA generation, and Q-PCR

Total RNA extraction, complementary DNA generation, and Q-PCR analyses were carried out as previously described (Moriyama *et al.*, 2012). Details of the primers used in these experiments are shown in Supplementary Table S2 online.

Western blot analysis

Western blot analysis was performed as previously described (Moriyama *et al.*, 2012; Moriyama *et al.*, 2013). Details are described in Supplementary Materials Online.

ChIP assay

The ChIP assay was performed using the SimpleChIP Enzymatic Chromatin IP Kit (Magnetic Beads) (Cell Signaling Technology, Danvers, MA) according to the manufacturer's instructions. Hemagglutinin-tagged Hes1 was immunoprecipitated with rabbit polyclonal antibody against hemagglutinin tag (ab9110, Abcam, Cambridge, MA). Immunoprecipitated DNA was analyzed by Q-PCR. Relative quantification using a standard curve method was performed, and the occupancy level for a specific fragment was defined as the ratio of immunoprecipitated DNA over input DNA. Details of the primers used in these experiments are shown in Supplementary Table S2 online.

Flow cytometry analysis

For autophagy detection, Cyto-ID Autophagy detection kit (Enzo Life Sciences, Plymouth Meeting, PA) was used according to the manufacturer's instructions. Details are described in Supplementary Materials Online.

CONFLICT OF INTEREST

The authors state no conflict of interest.

ACKNOWLEDGMENTS

We thank Shogo Nomura, Ayumi Kitagawa, and Riho Ishihama for technical support; Dr Takashi Ueno for helpful discussions; Dr Hiroyuki Miyoshi for the CSII-EF-RfA, pCMV-VSVG-RSV-Rev, and pCAG-HIVg/p plasmids; Dr Tamotsu Yoshimori for pEGFP-LC3 plasmid; and Dr Ryoichiro Kageyama for *Hes1* KO mice. This work was supported by MEXT KAKENHI grant 23791304 to MM. This work was also supported in part by grants from the Ministry of Health, Labor, and Welfare of Japan and a grant from the Program for Promotion of Fundamental Studies in Health Sciences of the National Institute of Biomedical Innovation (NIBIO).

SUPPLEMENTARY MATERIAL

Supplementary material is linked to the online version of the paper at http://www.nature.com/jid

REFERENCES

Aymard E, Barruche V, Naves T *et al.* (2011) Autophagy in human keratinocytes: an early step of the differentiation? *Exp Dermatol* 20:263–8

Bellot G, Garcia-Medina R, Gounon P *et al.* (2009) Hypoxia-induced autophagy is mediated through hypoxia-inducible factor induction of BNIP3 and BNIP3L via their BH3 domains. *Mol Cell Biol* 29:2570–81

Blanpain C, Lowry WE, Pasolli HA *et al.* (2006) Canonical notch signaling functions as a commitment switch in the epidermal lineage. *Genes Dev* 20:3022–35

Chan LL, Shen D, Wilkinson AR *et al.* (2012) A novel image-based cytometry method for autophagy detection in living cells. *Autophagy* 8:1371–82

Chatterjea SM, Resing KA, Old W *et al.* (2011) Optimization of filaggrin expression and processing in cultured rat keratinocytes. *J Dermatol Sci* 61:51–9

Diwan A, Krenz M, Syed FM *et al.* (2007) Inhibition of ischemic cardiomyocyte apoptosis through targeted ablation of Bnip3 restrains postinfarction remodeling in mice. *J Clin Invest* 117:2825–33

Feng X, Liu X, Zhang W *et al.* (2011) p53 directly suppresses BNIP3 expression to protect against hypoxia-induced cell death. *EMBO J* 30: 3397–415

Gilchrest BA, Soter NA, Stoff JS *et al.* (1981) The human sunburn reaction: histologic and biochemical studies. *J Am Acad Dermatol* 5:411–22

Hamacher-Brady A, Brady NR, Logue SE *et al.* (2007) Response to myocardial ischemia/reperfusion injury involves Bnip3 and autophagy. *Cell Death Differ* 14:146–57

Haruna K, Suga Y, Muramatsu S *et al.* (2008) Differentiation-specific expression and localization of an autophagosomal marker protein (LC3) in human epidermal keratinocytes. *J Dermatol Sci* 52:213–5

Ishibashi M, Moriyoshi K, Sasai Y *et al.* (1994) Persistent expression of helix-loop-helix factor HES-1 prevents mammalian neural differentiation in the central nervous system. *EMBO J* 13:1799–805

Itoh T, Itoh A, Pleasure D (2003) Bcl-2-related protein family gene expression during oligodendroglial differentiation. *J Neurochem* 85:1500–12

Juenemann K, Reits EA (2012) Alternative macroautophagic pathways. *Int J Cell Biol* 2012:189794

Kabeya Y, Mizushima N, Ueno T *et al.* (2000) LC3, a mammalian homologue of yeast Apg8p, is localized in autophagosome membranes after processing. *EMBO J* 19:5720–8

Knowles HJ, Athanasou NA (2008) Hypoxia-inducible factor is expressed in giant cell tumour of bone and mediates paracrine effects of hypoxia on monocyte-osteoclast differentiation via induction of VEGF. *J Pathol* 215:56–66

Lippens S, Denecker G, Ovaere P *et al.* (2005) Death penalty for keratinocytes: apoptosis versus cornification. *Cell Death Differ* 12(Suppl 2):1497–508

Mellor HR, Rouschop KM, Wigfield SM *et al.* (2010) Synchronised phosphorylation of BNIP3, Bcl-2 and Bcl-xL in response to microtubule-active drugs is JNK-independent and requires a mitotic kinase. *Biochem Pharmacol* 79:1562–72

Mizushima N, Levine B (2010) Autophagy in mammalian development and differentiation. *Nat Cell Biol* 12:823–30

Mizushima N, Yamamoto A, Matsui M *et al.* (2004) In vivo analysis of autophagy in response to nutrient starvation using transgenic mice expressing a fluorescent autophagosome marker. *Mol Biol Cell* 15:1101–11

Mizushima N, Yoshimori T, Levine B (2010) Methods in mammalian autophagy research. *Cell* 140:313–26

Moriyama H, Moriyama M, Sawaragi K *et al.* (2013) Tightly regulated and homogeneous transgene expression in human adipose-derived mesenchymal stem cells by lentivirus with tet-off system. *PLoS One* 8:e66274

Moriyama M, Durham AD, Moriyama H *et al.* (2008) Multiple roles of Notch signaling in the regulation of epidermal development. *Dev Cell* 14:594–604

Moriyama M, Moriyama H, Ueda A *et al.* (2012) Human adipose tissue-derived multilineage progenitor cells exposed to oxidative stress induce neurite outgrowth in PC12 cells through p38 MAPK signaling. *BMC Cell Biol* 13:21

Moriyama M, Osawa M, Mak SS *et al.* (2006) Notch signaling via Hes1 transcription factor maintains survival of melanoblasts and melanocyte stem cells. *J Cell Biol* 173:333–9

Nishida Y, Arakawa S, Fujitani K *et al.* (2009) Discovery of Atg5/Atg7-independent alternative macroautophagy. *Nature* 461:654–8

Ohtsuka T, Ishibashi M, Gradwohl G *et al.* (1999) Hes1 and Hes5 as notch effectors in mammalian neuronal differentiation. *EMBO J* 18:2196–207

Quinsay MN, Thomas RL, Lee Y *et al.* (2010) Bnip3-mediated mitochondrial autophagy is independent of the mitochondrial permeability transition pore. *Autophagy* 6:855–62

Rossiter H, Konig U, Barresi C *et al.* (2013) Epidermal keratinocytes form a functional skin barrier in the absence of Atg7 dependent autophagy. *J Dermatol Science* 71:67–75

Sassone J, Colciago C, Marchi P *et al.* (2010) Mutant Huntingtin induces activation of the Bcl-2/adenovirus E1B 19-kDa interacting protein (BNip3). *Cell Death Dis* 1:e7

Schweers RL, Zhang J, Randall MS *et al.* (2007) NIX is required for programmed mitochondrial clearance during reticulocyte maturation. *Proc Natl Acad Sci USA* 104:19500–5

Sowter HM, Ratcliffe PJ, Watson P *et al.* (2001) HIF-1-dependent regulation of hypoxic induction of the cell death factors BNIP3 and NIX in human tumors. *Cancer Res* 61:6669–73

Srinivas V, Bohensky J, Shapiro IM (2009) Autophagy: a new phase in the maturation of growth plate chondrocytes is regulated by HIF, mTOR and AMP kinase. *Cells Tissues Organs* 189:88–92

Tron VA, Trotter MJ, Tang L *et al.* (1998) p53-regulated apoptosis is differentiation dependent in ultraviolet B-irradiated mouse keratinocytes. *Am J Pathol* 153:579–85

Vengellur A, LaPres JJ (2004) The role of hypoxia inducible factor 1alpha in cobalt chloride induced cell death in mouse embryonic fibroblasts. *Toxicol Sci* 82:638–46

Walls KC, Ghosh AP, Ballestas ME *et al.* (2009) bcl-2/Adenovirus E1B 19-kd interacting protein 3 (BNIP3) regulates hypoxia-induced neural precursor cell death. *J Neuropathol Exp Neurol* 68:1326–38

Young AR (1987) The sunburn cell. *Photodermatology* 4:127–34

Zhang J, Ney PA (2009) Role of BNIP3 and NIX in cell death, autophagy, and mitophagy. *Cell Death Differ* 16:939–46

Zhao Y, Chen G, Zhang W *et al.* (2012) Autophagy regulates hypoxia-induced osteoclastogenesis through the HIF-1alpha/BNIP3 signaling pathway. *J Cell Physiol* 227:639–48

Zhao Y, Zhang CF, Rossiter H *et al.* (2013) Autophagy is induced by UVA and promotes removal of oxidized phospholipids and protein aggregates in epidermal keratinocytes. *J Invest Dermatol* 133:1629–37

STEM CELLS AND DEVELOPMENT
Volume 23, Number 18, 2014

DOI: 10.1089/scd.2013.0642

Role of Notch Signaling in the Maintenance of Human Mesenchymal Stem Cells Under Hypoxic Conditions

Hiroyuki Moriyama,[1,*] Mariko Moriyama,[1,*] Haruki Isshi,[1] Shin Ishihara,[1] Hanayuki Okura,[2] Akihiro Ichinose,[3] Toshiyuki Ozawa,[4] Akifumi Matsuyama,[2] and Takao Hayakawa[1]

Human adipose tissue-derived multilineage progenitor cells (hADMPCs) are attractive for cell therapy and tissue engineering because of their multipotency and ease of isolation without serial ethical issues. However, their limited in vitro lifespan in culture systems hinders their therapeutic application. Some somatic stem cells, including hADMPCs, are known to be localized in hypoxic regions; thus, hypoxia may be beneficial for ex vivo culture of these stem cells. These cells exhibit a high level of glycolytic metabolism in the presence of high oxygen levels and further increase their glycolysis rate under hypoxia. However, the physiological role of glycolytic activation and its regulatory mechanisms are still incompletely understood. Here, we show that Notch signaling is required for glycolysis regulation under hypoxic conditions. Our results demonstrate that 5% O_2 dramatically increased the glycolysis rate, improved the proliferation efficiency, prevented senescence, and maintained the multipotency of hADMPCs. Intriguingly, these effects were not mediated by hypoxia-inducible factor (HIF), but rather by the Notch signaling pathway. Five percent O_2 significantly increased the level of activated Notch1 and expression of its downstream gene, *HES1*. Furthermore, 5% O_2 markedly increased glucose consumption and lactate production of hADMPCs, which decreased back to normoxic levels on treatment with a γ-secretase inhibitor. We also found that HES1 was involved in induction of GLUT3, TPI, and PGK1 in addition to reduction of TIGAR and SCO2 expression. These results clearly suggest that Notch signaling regulates glycolysis under hypoxic conditions and, thus, likely affects the cell lifespan via glycolysis.

Introduction

HUMAN ADIPOSE TISSUE-DERIVED mesenchymal stem cells (MSCs), also referred to as human adipose tissue-derived multilineage progenitor cells (hADMPCs), are multipotent stem cells that can differentiate into various types of cells, including hepatocytes [1], cardiomyoblasts [2], pancreatic cells [3], and neuronal cells [4–6]. They can be easily and safely obtained from lipoaspirate without posing serious ethical issues and can also be expanded ex vivo under appropriate culture conditions. Moreover, MSCs, including hADMPCs, have the ability to migrate to injured areas and secrete a wide variety of cytokines and growth factors that are necessary for tissue regeneration [7–11]. In addition, due to their hypoimmunogenicity and immunomodulatory effects, hADMPCs are good candidates as gene delivery vehicles for therapeutic purposes [12]. Thus, hADMPCs are attractive seeding cells for cell therapy and tissue engineering. However, similar to other somatic stem cells or primary cells, hADMPCs have limited growth potential and ultimately stop proliferation as a result of cellular senescence [13], which hinders their therapeutic application.

Conversely, embryonic stem cells (ESCs) and induced pluripotent stem cells (iPSCs) are immortal under standard culture conditions. Recently, several groups have reported that these cells greatly rely on glycolysis for energy production even under high-oxygen conditions [14–16]. This phenomenon is known as the Warburg effect and was originally described for cancer cells by Otto Warburg in the 1920s [17]. Although mitochondrial respiration is more efficient than glycolysis in generating ATP (net yield of 30 ATPs vs. 2 ATPs), glycolysis is able to produce ATP considerably faster than mitochondrial respiration as long as glucose supplies are adequate. Thus, a metabolic shift from mitochondrial respiration to glycolysis would provide a growth advantage for actively proliferating cells. Moreover, Kondoh et al. demonstrated that enhanced glycolysis is also involved in cellular immortalization through reduction of

[1]Pharmaceutical Research and Technology Institute, Kinki University, Higashi-Osaka, Osaka, Japan.
[2]Platform of Therapeutics for Rare Disease and Health Policy, National Institute of Biomedical Innovation, Kobe, Japan.
[3]Department of Plastic Surgery, Kobe University Hospital, Kobe, Japan.
[4]Department of Dermatology, Graduate School of Medicine, Osaka City University, Osaka, Japan.
*These two authors contributed equally to this work.

intrinsic reactive oxygen species (ROS) production [14,18,19]. Since accumulation of intrinsic ROS levels could be a major reason for replicative senescence [20], enhancing glycolysis in cultured cells might improve the quality of the cells by suppressing premature senescence. One candidate method for induction of glycolysis is application of low-oxygen conditions to activate the transcription factor, hypoxia-inducible factor (HIF). HIF-1 is known to increase the expression of most glycolytic enzymes and the glucose transporters GLUT1 and GLUT3 [20]. Thus, several studies have reported that hypoxia is beneficial for the maintenance of hESCs in a pluripotent state [21,22]. Moreover, low oxygen tension has been reported to enhance the generation of iPSCs both from mouse and human primary fibroblasts [23].

Recently, hypoxic culture conditions have also been reported to confer a growth advantage, prevent premature senescence, and maintain undifferentiated states in somatic stem cells; for example, hematopoietic stem cells (HSCs) [24], neural stem cells [25], and bone marrow-derived MSCs [26]. These stem cells reside in their local microenvironments called the "stem cell niche," where the oxygen tension is relatively low (in the range of 1%–9%). Thus, hypoxic culture may be beneficial to these stem cells with regard to in vitro proliferation, cell survival, and differentiation. Takubo et al. reported that HSCs activated Pdk through HIF1α in hypoxic culture conditions, resulting in maintenance of glycolytic flow and suppression of the influx of glycolytic metabolites into mitochondria, and this glycolytic metabolic state was shown to be indispensable for the maintenance of HSCs [27]. Several studies have reported that MSCs exhibit a high level of glycolytic metabolism in the presence of high oxygen levels and further increase their rate of glycolysis on culture under hypoxia [28,29]. However, a relationship between beneficial effects of hypoxic conditions and metabolic status in addition to involvement of HIFs in the metabolic changes has not been investigated in these reports.

In this study, we aimed at investigating the effect of 5% oxygen on hADMPCs. Our results demonstrate that culture under 5% oxygen increased the glycolysis rate, improved the proliferation efficiency, prevented the cellular senescence, and maintained the undifferentiated status of hADMPCs. Intriguingly, these effects were not mediated by HIF, but rather by Notch signaling, an important signaling pathway required for the development of many cell types and maintenance of stem cells [30,31]. Five percent oxygen activated Notch signaling, resulting in the upregulation of *SLC2A3*, *TPI*, and *PGK1* in addition to the downregulation of *TIGAR* and *SCO2*, which may contribute to the increase in the glycolysis rate. These observations, thus, provide new regulatory mechanisms for stemness maintenance obtained under 5% oxygen conditions.

Materials and Methods

Adipose tissue samples

Subcutaneous adipose tissue samples (10–50 g each) were resected during plastic surgery from five female and two male patients (age 20–60 years) as discarded tissue. The study protocol was approved by the Review Board for Human Research of Kobe University Graduate School of Medicine Foundation for Biomedical Research and Innovation, Osaka City University Graduate School of Medicine, and Kinki University Pharmaceutical Research and Technology Institute (reference number: 12-043). Each subject provided signed informed consent.

Cell culture

hADMPCs were isolated as previously reported [11,32–34] and maintained in a medium containing 60% DMEM low glucose, 40% MCDB-201 medium (Sigma Aldrich), 1× insulin-transferrin-selenium (Life Technologies), 1 nM dexamethasone (Sigma Aldrich), 100 mM ascorbic acid 2-phosphate (Wako), 10 ng/mL epidermal growth factor (PeproTech), and 5% fetal bovine serum. The cells were plated to a density of 5×10^3 cells/cm^2 on fibronectin-coated dishes, and the medium was replaced every 2 days. For hypoxic culture, cells were cultured in a gas mixture composed of 90% N_2, 5% CO_2, and 5% O_2. For maintenance of the hypoxic gas mixture, a ProOx C21 carbon dioxide and oxygen controller and a C-Chamber (Biospherix) were used.

Senescence-associated β-galactosidase staining

Cells were fixed with 2% paraformaldehyde/0.2% glutaradehyde for 5 min at room temperature and then washed twice with phosphate-buffered saline (PBS). The cells were then incubated overnight at 37°C with fresh senescence-associated β-galactosidase (SA-β-Gal) chromogenic substrate solution (1 mg/mL Bluo-gal (Life Technologies), 40 mM citric acid (pH 6.0), 5 mM potassium ferrocyanide, 5 mM potassium ferricyanide, 150 mM NaCl, and 2 mM $MgCl_2$).

Measurement of ROS production

Cells were harvested and incubated with 10 μM 5-(and-6)-chloromethyl-2′,7′-dichlorodihydrofluorescein diacetate, acetyl ester (CM-H_2DCFDA). The amount of intracellular ROS production was proportional to the green fluorescence, as analyzed using a Guava EasyCyte 8HT flow cytometer (Millipore) using an argon laser at 488 nm and a 525/30 nm band pass filter, and dead cells were excluded using the Live/Dead Fixable Far Red Dead Cell Stain Kit (Life Technologies).

EdU proliferation assay

For assessment of cell proliferation, hADMPCs were seeded on a fibronectin-coated six-well plate at a density of 5×10^3 cells/cm^2 and cultured for 3 days. Cell proliferation was detected by incorporating of 5-ethynyl-2′-deoxyuridine (EdU) and using the Click-iT EdU Alexa Fluor 488 Flow Cytometry Assay Kit (Life Technologies). Briefly, according to the manufacturer's protocol, cells were incubated with 10 μM EdU for 2 h before fixation, permeabilized, and stained with EdU. EdU-positive cells were then analyzed using the 488 nm laser of a Guava EasyCyte 8HT flow cytometer (Millipore).

Flow cytometry analysis

Flow cytometry analysis was performed as previously described [34]. Briefly, hADMPCs were harvested and resuspended in staining buffer (PBS containing 1% BSA, 2 mM EDTA, and 0.01% sodium azide) at a density of

1×10^6 cells/mL, incubated for 20 min with a fluorescein isothiocyanate (FITC)-conjugated antibody against CD49b or CD98 (BioLegend) or a phycoerythrin (PE)-conjugated antibody against CD10, CD13, CD29, CD44, CD49a, CD49c, CD49d, CD49e, CD51/61, CD73, CD90, CD105, CD117, SSEA4, HLA-A,B,C (BioLegend), CD133/1 (Miltenyi Biotec), or CD166 (Beckman Coulter). Nonspecific staining was assessed using relevant isotype controls. Dead cells were excluded using the Live/Dead Fixable Far Red Dead Cell Stain Kit (Life Technologies). FlowJo software was used for quantitative analysis.

RNA extraction, cDNA generation, and quantitative polymerase chain reaction

Total RNA was extracted using the RNeasy Mini Kit (Qiagen) accroding to the manufacturer's instructions. cDNA was generated from 1 μg of total RNA using the Verso cDNA Synthesis Kit (Thermo Scientific) and purified using the MinElute PCR Purification Kit (Qiagen). Quantitative polymerase chain reaction (Q-PCR) analysis was conducted using the SsoFast EvaGreen supermix (Bio-Rad) according to the manufacturer's protocols. The relative expression value for each gene was calculated using the ΔΔCt method, and the most reliable internal control gene was determined using geNorm Software (http://medgen.ugent.be/~jvdesomp/genorm/). Details of the primers used in these experiments are available on request.

Western blot analysis

Whole cell extracts were prepared by washing cells with ice-cold PBS and lysing them with M-PER Mammalian Protein Extraction Reagent (Thermo Scientific Pierce) according to the manufacturer's instructions. Nuclear and cytosolic extracts were prepared as follows. Cells were washed with ice-cold PBS and lysed with lysis buffer (50 mM Tris-HCl (pH 7.5), 0.5% Triton X-100, 137.5 mM NaCl, 10% glycerol, 5 mM EDTA, 1 mM sodium vanadate, 50 mM sodium fluoride, 10 mM sodium pyrophosphate, and protease inhibitor cocktail). Then, insoluble nuclei were isolated by centrifugation and lysed with lysis buffer containing 0.5% SDS. Equal amounts of proteins were separated by sodium dodecyl sulfate polyacrylamide gel electrophoresis (SDS-PAGE), transferred to polyvinylidene fluoride membranes (Immobilon-P; Millipore), and probed with antibodies against cleaved Notch1 (#2421; Cell Signaling Technology), HIF-1α (#610959; BD Bioscience), hypoxia-inducible factor 2α (MAB3472; Millipore), Akt (#9272; Cell Signaling Technology), and phospho Akt (Ser473) (#4060; Cell Signaling Technology). Horseradish peroxidase (HRP)-conjugated anti-mouse or -rabbit IgG antibody (Cell Signaling Technology) was used as a secondary antibody, and immunoreactive bands were visualized using Immobilon Western Chemiluminescent HRP substrate (Millipore). The band intensity was measured using the ImageJ software.

Fluorescence microscopy

Phase-contrast and fluorescence images were obtained using a fluorescence microscope (BZ-9000; Keyence) using BZ Analyzer Software (Keyence).

Adipogenic, osteogenic, and chondrogenic differentiation procedures

For adipogenic differentiation, cells were cultured in differentiation medium (Zen-Bio). After 7 days, half of the medium was exchanged for adipocyte medium (Zen-Bio) and this was repeated every 3 days. Three weeks after differentiation, adipogenic differentiation was confirmed by a microscopic observation of intracellular lipid droplets with the aid of Oil Red O staining. Osteogenic differentiation was induced by culturing the cells in osteocyte differentiation medium (Zen-Bio). Differentiation was examined by Alizarin Red staining. For chondrogenic differentiation, 2×10^5 hADMSCs were centrifuged at 400 *g* for 10 min. The resulting pellets were cultured in chondrogenic medium (Lonza) for 21 days. The pellets were fixed with 4% paraformaldehyde in PBS, embedded in OCT, frozen, and sectioned at 8 μm. The sections were incubated with PBSMT (PBS containing 0.1% Triton X-100, and 2% skim milk) for 1 h at room temperature, and then incubated with a mouse monoclonal antibody against type II collagen (Abcam) for 1 h. After washing with PBS, cells were incubated with Alexa 546-conjugated anti-mouse IgG to identify chondrocytes (Life Technologies). The cells were counterstained with 4′-6-diamidino-2-phenylindole (DAPI) (Life Technologies) to identify cellular nuclei. The sections were also stained with 1% alcian blue (Sigma Aldrich) in 3% acetic acid, pH 2.5 for 30 min.

Determination of HK, PFK, LDH, PDH, and Cox IV activities

Cells (2×10^6) were lysed, and HK, PFK, LDH, or PDH activity was measured using the Hexokinase Colorimetric Activity Kit, Phosphofructokinase (PFK) Activity Colorimetric Assay Kit, Lactate Dehydrogenase (LDH) Activity Assay Kit, or Pyruvate Dehydrogenase Activity Colorimetric Assay Kit (all from BioVision), respectively, according to the manufacturer's instructions. To measure Cox IV activity, mitochondria were isolated from 2×10^7 cells using a Mitochondria Isolation Kit (Thermo Scientific) and lysed with buffer containing n-Dodecyl β-D-maltoside, followed by measurement with the Mitochondria Activity Assay (Cytochrome C Oxidase Activity Assay) Kit (BioChain Institute), according to the manufacturer's instructions.

Results

5% oxygen hypoxic culture condition increases proliferation capacity and decreases senescence

hADMPCs were cultured under 20% oxygen (normoxia; Nx) or 5% oxygen (hypoxia; Hx), and their proliferation capacities were examined based on the relationship between the number of cultivation days and the population doubling level (PDL). Nx-cultured hADMPCs ceased proliferation at a PDL of 35–40 (between 46–70 days), whereas continuous cell proliferation beyond 45 PDL was observed when hADMPCs were cultured in the Hx condition (Fig. 1A). To investigate whether this increase of PDL in the Hx culture condition resulted from an increase in cell cycle progression and increase in survival rates, EdU, an alternative to 5-bromo-2′-deoxyuridine (BrdU), was incorporated into the

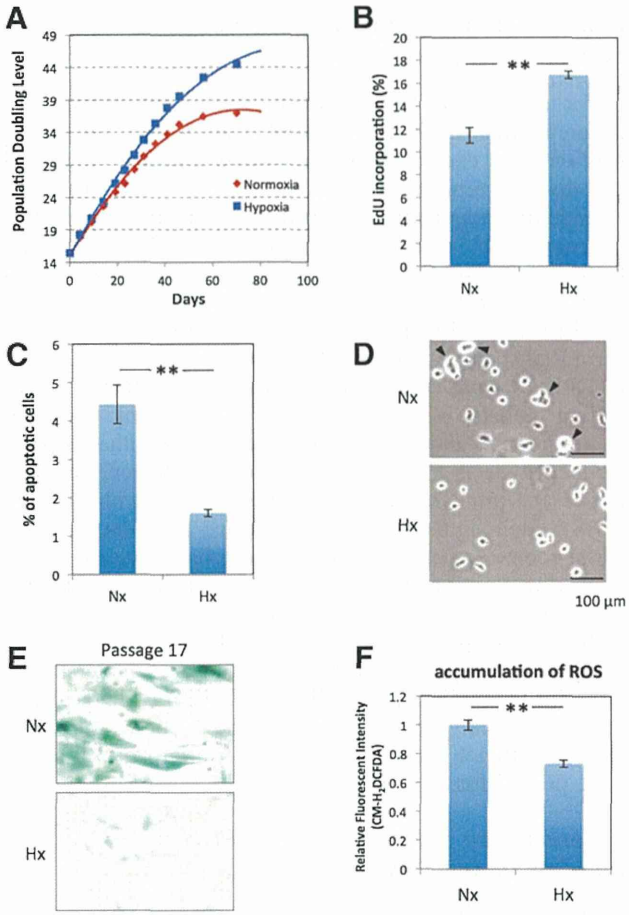

FIG. 1. Hypoxia increases proliferation capacity and decreases senescence in tissue-derived multilineage progenitor cells (hADMPCs). **(A)** Growth profiles of hADMPCs under normoxic (*red square*) and hypoxic (*blue square*) conditions. The population doubling level (PDL) was determined to be 0 when cells were isolated from human adipose tissue. Cells were maintained until they reached PDL13–15 (passage 3) and then split into four aliquots of equal cell densities. PDL was calculated based on the total cell number at each passage. **(B)** Detection of normoxic (Nx) and hypoxic (Hx) cells by flow cytometry after incorporation of EdU. **(C)** Percentages of apoptotic cells with sub-G1 DNA under Nx and Hx conditions. The results are presented as the mean of three independent experiments. **(D)** hADMPCs cultured under Nx and Hx conditions were harvested by trypsin-EDTA and then imaged using a phase-contrast microscope. *Arrowheads* indicate cells with a larger and more irregular shape. **(E)** Cells expanded under Nx and Hx conditions were stained with SA-β-gal. **(F)** Cellular reactive oxygen species detection by the oxidative stress indicator CM-H_2DCFDA in hADMPCs under Nx or Hx. Data are presented as the mean fluorescence intensity of three independent experiments. Error bars indicate SD. $^{**}P < 0.01$ indicates significant difference (independent *t*-test) between Nx and Hx. Scale bars; 100 μm. Color images available online at www.liebertpub.com/scd

genomic DNA of the hADMPCs, and the amount of incorporated EdU was quantified by flow cytometry. As shown in Fig.1B, the EdU incorporation rate was significantly higher in Hx-cultured hADMPCs than in Nx-cultured hADMPCs, suggesting that cell growth was increased in the Hx culture condition. In addition, measurement of DNA content in hADMPCs revealed a slight but significant decrease of sub-G1 peaks, which indicates the existence of apoptotic cells with degraded DNA, when the cells were cultured in the Hx condition (Fig. 1C). These data suggest that the Hx culture condition increases the proliferation capacity of hADMPCs by promoting their cell growth and survival rates. We also found that Nx-cultured hADMPCs were larger with a more irregular shape (Fig. 1D), which suggests that the Hx culture condition prevented hADMPCs from entering senescence [35]. To further investigate this phenomenon, cellular senescence was measured by staining for SA-β-Gal, which revealed that SA-β-Gal activity was increased in Nx-cultured hADMPCs at passage 17 (Fig. 1E). Since it has been hypothesized that senescence results from oxidative stress [20], accumulation of ROS in hADMPCs was detected using the nonfluorescent probe, CM-H_2DCFDA. Flow cytometry analysis revealed that ROS were generated at higher levels in hADMPCs when cultured in the Nx condition (Fig. 1F), suggesting that reduced production of ROS in the Hx condition may prevent the cells from entering replicative senescence.

Hypoxic culture maintains some MSC properties and increases differentiation

We then examined the cell properties of hADMPCs under Nx and Hx conditions. Initially, cell surface antigens expressed on hADMPCs were analyzed by flow cytometry. No significant difference in expression profile between hADMPCs cultured in Nx and Hx was observed; the cells were consistently positive for CD10, CD13, CD29, CD44, CD49a, CD49b, CD49c, CD49d, CD49e, CD51/61, CD54, CD59, CD73, CD90, CD98, CD105, CD166, and HLA-A, B, C, but negative for CD34, CD45, CD117, and CD133 (Fig. 2 and data not shown). These data were consistent with previous reports describing the expression profiles of cell surface markers of hMSCs [36,37]. To further examine the stem cell properties of hADMPCs, their potential for differentiation into adipocyte, osteocyte, and chondrocyte lineages was analyzed at passage 8. Hx-cultured hADMPCs presented enhanced differentiation into various lineages (Fig. 3A, B), indicating that the Hx culture condition improved the stem cell properties of hADMPCs.

Hypoxic culture condition activates Notch signaling

To reveal the molecular mechanism by which the Hx culture condition increased the proliferative capacity and maintained the stem cell properties of hADMPCs, we next examined Notch signaling, which is required for maintaining stem-cell features of various types of stem cells [30,31]. As expected, levels of cleaved NOTCH1, an activated form of NOTCH1, were significantly increased (greater than twofold) in the Hx culture condition (Fig. 4A). Q-PCR analysis revealed that HES1, a downstream target of Notch signaling, was upregulated in Hx-cultured hADMPCs, which also indicated that Notch signaling was activated in